11 Further Manifestations of Depletion Effects

In this chapter we provide examples of the manifestations of depletion effects in areas such as biology and technology. The addition of nonadsorbing polymers to colloidal suspensions can cause phase separation of the mixture into a colloid-rich and a polymer-rich phase. The understanding of this polymer-induced phase separation is very important, not only for colloid science but also for industrial systems, such as food dispersions [1–4] and paint [5–8]. Colloids and polymers (or surfactants) are both present in these systems and influence the stability and subsequent processing issues. This holds similarly for binary or multi-component colloidal mixtures.

It has been realised that procedures employing the depletion interaction have the potential to enable the fabrication of materials based on self-organised colloidal structures [9]. Adding depletants can for instance enable the formation of a Penrose quasi-crystal of mobile colloidal tiles [10].

Also, the importance of depletion effects in biological systems is recognised [11–15]. Nonadsorbing polymer chains promote the adhesion of cells to surfaces [16] and enhance adsorption of lung surfactants at the air–water interface in lungs so as to help patients suffering from acute respiratory syndrome [17]. The physical properties of actin networks are affected by nonadsorbing polymers [18], which also modify phase transitions in virus dispersions [19]. It has been shown that depletion forces can deform epithelial cells [20]. Rod-like depletants are even able to induce a plethora of shape transitions of red blood cells. To further illustrate this, we discuss a few examples of depletion effects in systems of biological and technological interest in this chapter.

H. N. W. Lekkerkerker, R. Tuinier, M. Vis, *Colloids and the Depletion Interaction*,
Lecture Notes in Physics 1026, https://doi.org/10.1007/978-3-031-52131-7_11

11.1 Macromolecular Crowding

A longstanding question in molecular biology is the extent to which the behaviour of macromolecules observed in vitro accurately reflects their behaviour *in vivo* [21]. A characteristic of the cytoplasm of living cells is the high concentration of macromolecules (including proteins and nucleic acids) that they contain (up to 400 g/L) [22,23]. Since the 1980s [22,24,25] it has been increasingly appreciated that the large volume fraction occupied by these macromolecules influences several intracellular processes [26–28], ranging from the bundling of biopolymers like DNA and actin, to the phase separation in a bacterial cell. These effects are known amongst biochemists and biophysicists as *macromolecular crowding* (see for instance Refs. [11,15,29–32]). The term 'crowding' is used rather than 'concentrated' because, in general, no single macromolecular species occurs at high concentration but, taken together, the macromolecules occupy a significant fraction (typically 10–30%) of the total volume [33].

The biological relevance of crowding such as chemical equilibria and rates, association reactions and enzyme kinetics has been studied extensively. For reviews, see Refs. [26,33]. Another important characteristic where macromolecular crowding plays an important role is phase separation in the cytoplasm. Walter and Brooks [34] put forward the hypothesis that macromolecular crowding is the basis for microcompartmentalisation.

Phase separation between a nucleoid and cytoplasm in bacterial cells is a striking example of macromolecular crowding [35–37]. Chromosomes in bacterial cells do not occur in dispersed form but are organised in the nucleoid as a separate phase. Depletion forces that originate from the presence of proteins can explain the phase separation [36]. As a result, the proteins partition over the cytoplasm and nucleoid phases. Their concentration in the cytoplasm is about two times larger than their concentration in the nucleoid phase [37] (see Fig. 11.1).

Another example where macromolecular crowding plays a key role is fluid–fluid phase separation in the cell [15,38–46]. Here, phase transitions give rise to dense droplets in the cell such as nucleoli, germ granules and speckles [43,45] that have been collectively described as membraneless organelles. This is schematically illustrated in Fig. 11.2 [15].

There has been significant interest in the role that the depletion interaction plays in driving cellular organisation [11–13,47,48]. However, while the depletion interaction promotes fluid–fluid phase separation in the cell, Groen et al. [48] have argued that crowded macromolecular solutions are very prone to non-specific associative interactions that can potentially counteract depletion. It gradually becomes clear that excluded volume interactions can explain the assembly of, and liquid–liquid phase separation in, a wide range of cellular structures. These range from the cytoskeleton to chromatin loops and entire chromosomes [11,15].

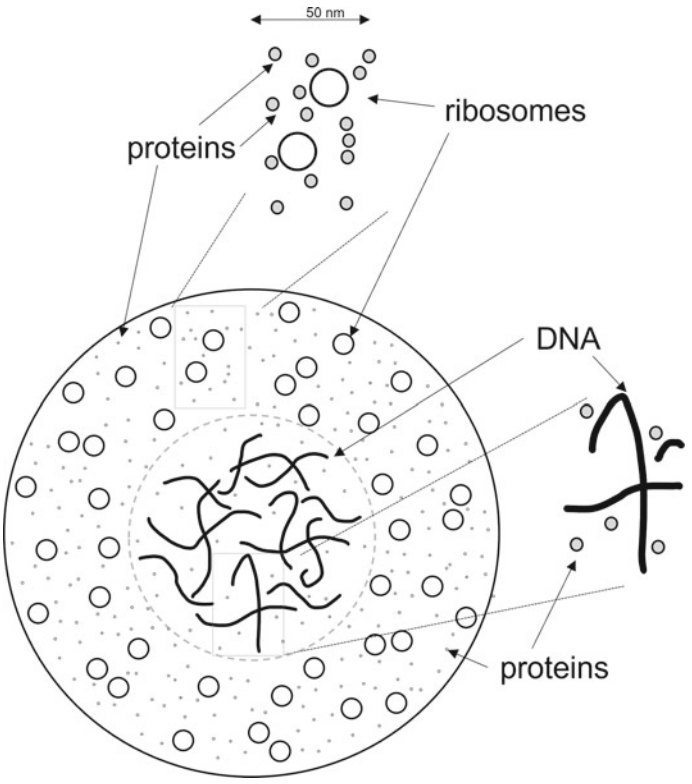

Fig. 11.1 Representation of a bacterial cell containing phase-separated nucleoid and cytoplasm. DNA is concentrated in the nucleoid, and ribosomes and proteins are concentrated in the cytoplasm. Inspired by a drawing in Ref. [37]

11.2 Depletion Interactions and Protein Crystallisation

In 1934, Desmond Bernal and Dorothy Crowfoot (later Hodgkin) discovered that crystals of the digestive enzyme pepsin give a well-resolved X-ray diffraction pattern [49]. It took 25 years before the first atomic structures of proteins using X-ray crystallography were determined. In 1958 Kendrew et al. published the structure of the protein myoglobulin [50], which stores oxygen in muscle cells; and in 1960, Perutz et al. [51] reported the structure of the protein haemoglobin, which transports oxygen in blood.

The first requirement for protein structure determination with X-ray diffraction is to grow suitable crystals [52]. While great strides have been made in the determination of protein structures (more than 200,000 protein structures have been resolved [53]), protein crystallisation (notwithstanding a history spanning more than 150 years [54, 55]) remains somewhat elusive. This actually holds for crystallisation in general [56].

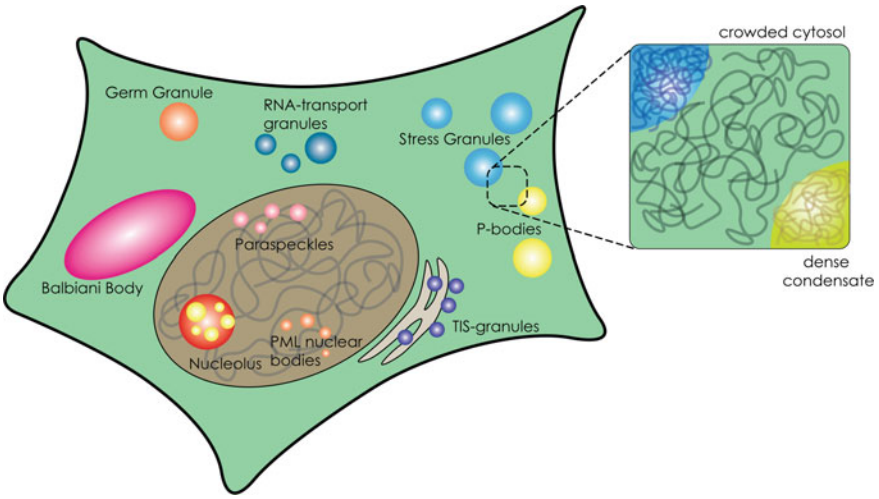

Fig. 11.2 A eukaryotic cell containing several types of organelles. *Inset*: the crowded state of the cytosol. Reprinted from Ref. [15] under the terms of CC-BY-4.0

Figure 11.3 characterises the state of the art in protein crystallisation in 1988 [57]. In recent years, significant progress has been made in understanding protein crystallisation on the basis of the phase diagram of protein solutions. The key observation that lies at the basis of this development was made by Benedek and co-workers [58,59]. In the course of their investigations of proteins involved in maintaining the transparency of the eye lens, they discovered that in aqueous solutions of several bovine lens proteins the solid-liquid phase boundary lies higher in temperature than the liquid–liquid coexistence curves. Thus, over a range of concentrations and temperatures for which liquid–liquid phase separation occurs, the coexistence of a protein crystal phase with a protein liquid solution phase is thermodynamically stable relative to the metastable separated liquid phases [60] (Fig. 11.4). Note also the metastable critical fluid–fluid point [58,59,61–65].

It was shown that this remarkable phase behaviour could be understood on the basis of the sensitivity to the form of the pair potential of the phase diagram of small attractive colloidal particles [66–69]. Moreover, it was soon realised that successful protein crystallisation depends on the location (protein concentration and temperature) in the phase diagram [65,70–74]. Control of protein crystal nucleation around the metastable 'liquid–liquid' phase boundary [74] appears key to the development of systematic crystallisation strategies (for a concise review, see Ref. [75]). This phase boundary can be manipulated by depletion interactions through the addition of nonadsorbing polymers such as polyethylene glycol [76–78].

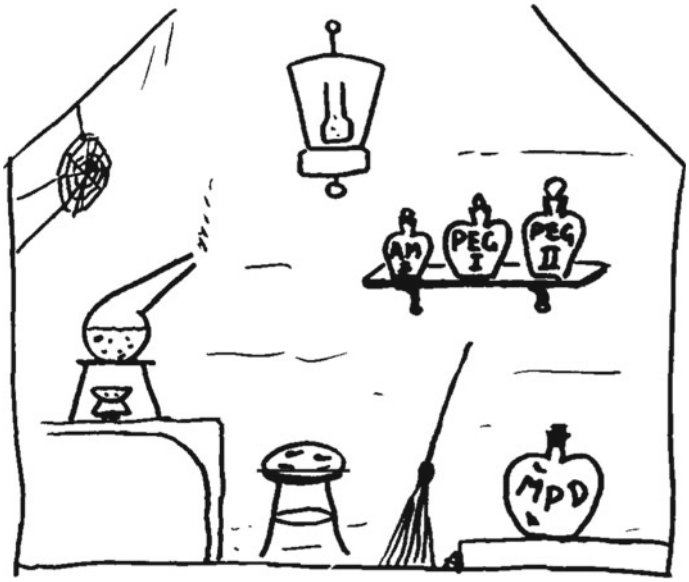

Fig. 11.3 View upon the 'art' of protein crystallisation by J. Drenth. Reprinted with permission from Ref. [57]. Copyright 1988 Elsevier

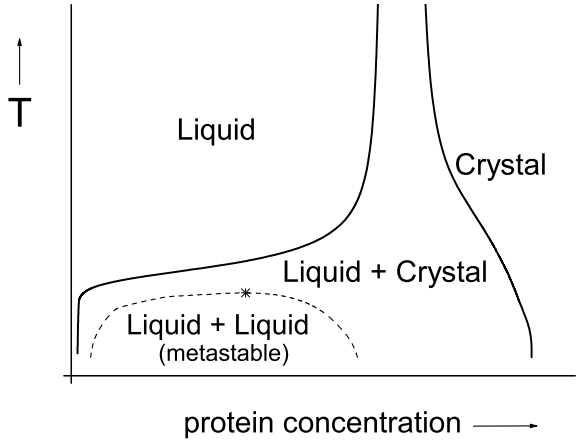

Fig. 11.4 Typical phase diagram of a globular protein solution. The critical point is marked by the asterisk

Exercise 11.1. Argue how Fig. 11.4 is modified upon increasingly adding nonadsorbing polymers for $q > 0.3$.

To illustrate the role of nonadsorbing polymer chains on the protein solution phase behaviour, we discuss the results of adding PEG to a solution with the protein apoferritin by Tanaka and Ataka [79]. Apoferritin is an iron storage protein consisting of 24 subunits. The effective radius is about 8 nm and the molar mass of apoferritin is 440 kg/mol. It is not easy to crystallise a solution of apoferritins by adding salt ions. Traditionally, a well-defined scale known as the Hofmeister series [80] is used as a measure for the efficiency of precipitating proteins. A solution of apoferritin cannot be crystallised in the common manner with the usual salt ions as precipitating agents. Adding PEG, however, does make it possible to induce crystallisation. Fig. 11.5 shows the experimental data obtained from visual and microscopic inspection of PEG–apoferritin in aqueous 0.6 M NaCl solutions. The concentration of apoferritin was fixed at 54 g/L. The PEG concentration and molar mass were varied. Four molar masses M_{PEG} (and radii of gyrations R_{g}) of the PEGs were used: 1.5, 4.0, 8.0 and 20 kg/mol (1.4, 2.5, 3.7 and 6.2 nm, respectively), corresponding to $q = 0.18, 0.31, 0.46,$ and 0.78.

Various situations were observed after mixing PEG with apoferritins [79]. For sufficiently small concentrations (depending on M_{PEG}, hence q) the mixture was stable (△, Fig. 11.5), while further increasing the PEG concentration leads to a phase transition. At $q = 0.18$ random aggregates (•) were found, which is typical for a protein solution undergoing a fluid-to-solid transition and does not give the proper conditions for obtaining good-quality crystals. The same happens for the highest concentrations at $q = 0.31$ and 0.46. For $q = 0.31, 0.46,$ and 0.78 there was a region where liquid domains (+) were formed, indicative of a gas–liquid phase transition, usually referred to as liquid–liquid phase separation. For $q = 0.78$, liquid domains were found in the entire unstable regime. Finally, good-quality crystals (○), in coexistence with liquid domains, were formed at $q = 0.31$ and 0.46 for intermediate PEG concentrations. For these q-values the critical point is close to the fluid–crystal coexistence line, in agreement with the findings of Ten Wolde and Frenkel [71]. Thus, it follows that adding PEG indeed provides the conditions for good crystallisation within a specific range of protein–polymer size ratios and polymer concentrations. The different states are illustrated with the micrographs in the right panel of Fig. 11.5.

Aided crystallisation is, of course, not limited to proteins. For instance, Kirner and Sturm [81] used depletant-mediated crystallisation to separate mixtures of nanocrystals of different sizes and shapes.

11.3 Shape and Size Selection

The depletion interaction, as argued in Sect. 1.2.5, depends on the concentration of the depletion agent and the overlap volume of the depletion zones. For a given concentration of depletant the only variable is the overlap volume, which in turn depends on the size (see Chap. 2) and shape of the colloidal particles. Tuning the strength of the depletion interaction therefore allows particles of different size and shape to be separated. For example, the separation of rod-like particles and spheres under the influence of polymers is schematically indicated in Fig. 11.6.

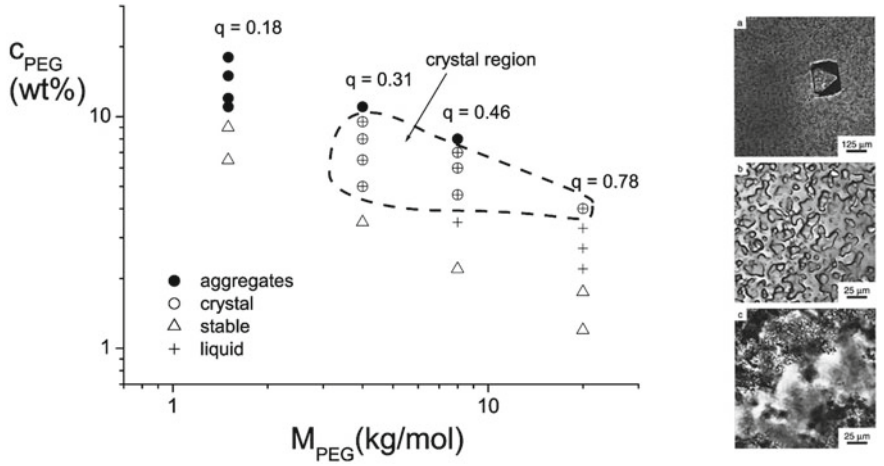

Fig. 11.5 Phase behaviour of apoferritin with PEG. *Left*: state diagram of apoferritin mixed with PEG of various molar masses. The apoferritin concentration was kept constant at 54 g/L and the molar mass and concentration of PEG was varied as indicated in the diagram. Results are redrawn from Ref. [79]. *Right*: Micrographs representing the various kinds of unstable solutions that were found in aqueous apoferritin–PEG mixtures: **a** crystals, **b** liquid domains and **c** random aggregates. Right panel: reprinted with permission from Ref. [79]. Copyright 2002, American Institute of Physics

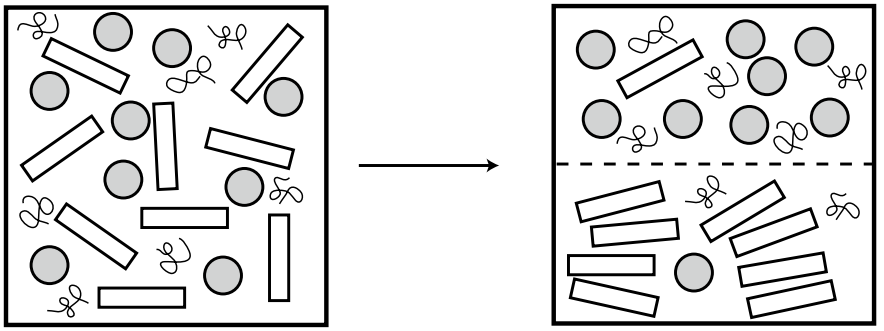

Fig. 11.6 Shape-selective separation induced by depletion forces

Unaware of the underlying principle, this had already been used by Cohen in 1941 [82] to separate two viruses, Tobacco Mosaic Virus and Tobacco Necrosis Virus. Tobacco Mosaic Virus is a rod-like virus with a length of 300 nm and diameter of 18 nm, and Tobacco Necrosis Virus a spherical virus with a diameter of about 26 nm. Cohen used the polysaccharide heparin as depletant to separate these viruses. This method to separate colloids of different sizes and shapes has recently gained new impetus. Obtaining particles of a specific size and shape is critical for optimising the nanostructure-dependent optical, electrical and magnetic properties in nano-based technologies.

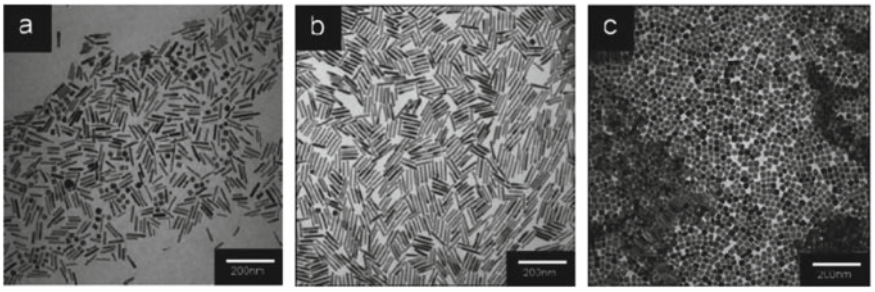

Fig. 11.7 TEM images of a dispersion of rod-like and cube-like gold colloids. **a** synthesised mixture, **b** sediment, **c** supernatant. Reprinted with permission from Ref. [86]. Copyright 2010, American Chemical Society (ACS)

While the self-organisation of nearly monodisperse spherical colloidal particles has been studied for a long time, the full potential of the self-assembly of anisometric colloidal particles (rods and plates) is far from being achieved. Nevertheless, important advances have been made. For example, CdSe semiconductor nanorods have been shown to form nematic liquid crystals [83] that can potentially be used as functional components in electro-optical devices. Kim et al. [84] succeeded in generating long-range assembly of colloidal anisotropic nanocrystals into thin films with orientational and positional order by adding depletants. Hence, the depletion interaction has the potential to enable the effective separation of anisometric colloids from a mixture of particles of different sizes and shapes.

Depletion-induced shape and size selection of colloidal particles could be a powerful tool to achieve the separation of different components. For instance, efficient purification of gold platelets in complex multi-component colloidal mixtures was realised by Zhao et al. [85] using surfactant micelles as depletants. Park et al. [86] reported the depletion-induced shape and size selection of gold rods and cubes. In Fig. 11.7 we show their transmission electron microscopy (TEM) images of gold rods ($L = 77\,\text{nm}$, $D = 11\,\text{nm}$) and cubes (20 nm), which could be separated by adding nonadsorbing polymers.

Baranov et al. [9] showed that the depletion attraction forces were effective in the shape selective separation of CdSe/CdS-rods from a mixture of rods and CdSe spheres. Mason [87] showed that the depletion interaction between plate-like particles is much stronger than between spheres, leading to a separation between a phase enriched with plates and a phase mainly concentrated with spheres. The dependence of the depletion interaction on size can also be used to fractionate a bidisperse population of colloidal spheres [88], or to obtain a monodisperse population of spheres from a collection of polydisperse spheres [89]. Bidisperse colloidal particle mixtures have the potential to self-organise into colloidal crystals (see Chap. 6 for more details).

Ye et al. [90] presented an experimental-computational investigation of mixtures of rods and spheres showing that the mixture can co-assemble into a binary superlattice. The formation of two-dimensional colloidal membranes from a suspension of rod-like viruses mixed with nonadsorbing polymer chains was studied by Kang

et al. [91]. It is clear that depletion forces can be exploited in the design of a wide range of reconfigurable colloidal structures.

These procedures, based on the depletion interaction, have the potential to enable powerful fabrication procedures of materials based on self-organised colloidal structures. A computational study by Bevan et al. [92] showed that actuating colloidal assembly in a practical process is feasible, and they provided insights into how to optimise the process conditions.

11.4 Directing Colloidal Self-assembly Using Surface Microstructures

As indicated in Sect. 11.3, the depletion interaction depends on the overlap volume for a given depletant concentration. This dependence leads to a difference in depletion interaction between particles of different sizes and shapes and offers a powerful and cost-effective way to separate them.

The use of surface microstructures provides a promising route for creating colloidal assemblies via depletion forces. Dinsmore, Yodh and Pine [93] studied the interaction of large polystyrene spheres ($R = 203$ nm, $\phi = 10^{-5}$) in a sea of small polystyrene spheres ($R = 41$ nm, $\phi = 0.30$) with a wall with a step edge, see Fig. 11.8.

Clearly, the overlap volume depends on the position of the big sphere with respect to the step edge. Since the depletion interaction can be seen as the product of overlap volume and osmotic pressure of the depletants ($W_{\text{dep}} \approx -PV_{\text{ov}}$, where P is now the osmotic pressure of the small spheres (see Eq. 1.18)), a difference in overlap volume affects the depletion interaction accordingly. It is, therefore, also expected that confinement effects can mediate phase transitions [94,95]. Spannuth and Conrad

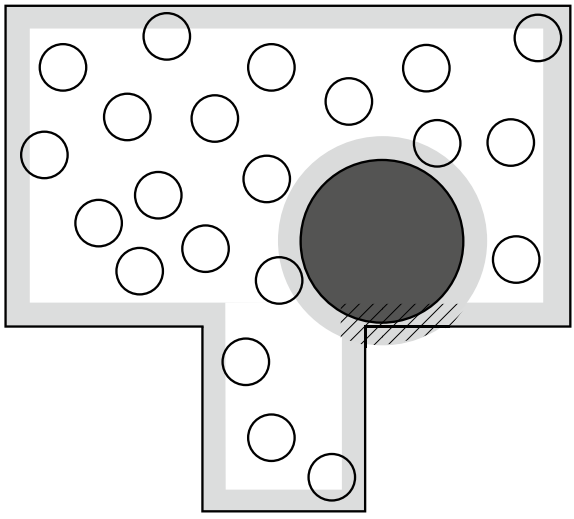

Fig. 11.8 A large colloidal sphere near a step edge in a sea of small spheres. The presence of the small spheres leads to depletion zones (light grey regions) near the walls of the container and around the big sphere. Overlap of depletion zones is indicated by the hatched area. This overlap volume increases the volume accessible to the small spheres, thereby increasing their entropy

showed that confinement of a colloid–polymer mixture can induce solidification [96]. For an overview of theoretical accounts on confinement and depletion effects, see Ref. [97]. Confinement effects are also relevant for the microchannel flow of colloidal or colloid–polymer mixtures [94,98].

The depletion interaction can be derived by measuring the probability of the various positions (h) of the big particles on the terrace with the step edge using optical microscopy, and relating this probability $p(h)$ with the Boltzmann relation

$$p(h) \sim \mathrm{e}^{-W_{\mathrm{dep}}(h)/kT}, \tag{11.1}$$

the depletion interaction can be measured. For the system, the differences in the overlap volume amount to a difference in the depletion potential of about twice the thermal energy of the particles. This indicates that surface structures can create localised force fields that can trap particles.

Exercise 11.2. Rationalise what are more favourable positions inside the box for the big sphere in Fig. 11.8.

An interesting application of this concept can be found in the work of Sacanna et al. [99]. By clever colloid synthesis, they created 5 μm (diameter) polymerised silicon oil droplets with a well-defined spherical cavity. To these 'lock' particles they added appropriately sized spherical 'key' particles (silica, poly(methyl methacrylate) or polystyrene colloids) that can fit into the cavity. Nanometer sized nonadsorbing polymers were added to provide a depletion interaction. The depletion interaction, being proportional to the overlap volume of the depletion zones, attains a maximum when the key particle fits precisely into the spherical cavity of a lock particle (Fig. 11.9). The depletion-driven self-assembly of lock-and-key particles is demonstrated in Fig. 11.10. This time series (from left to right) illustrates the site-specificity of the attraction.

By developing colloids with well-defined multicavities, this concept has been extended to make lock particles with multiple key holes [101]. Adding appropriately sized depletants to dispersions of colloidal golf-balls [102] induces the formation of controlled self-assembled structures. Computer simulations have shown how the binding tendency in a dispersion of lock-and-key colloids can be controlled by adjusting the characteristics of polymeric depletants [103]. Theoretical predictions revealed interesting phase behaviour of such mixtures of lock-and-key particles with depletants [104].

Another way to manipulate the overlap volume of the depletion zones is to vary the roughness of the surface [105] of the colloidal particles (Fig. 11.11). The left drawings show that surface roughness does not affect the overlap volume for intermediate overlap of depletion zones. When the particles are in close contact surface roughness prevents overlap of certain zones that would normally overlap for smooth surfaces (see the sketches on the right).

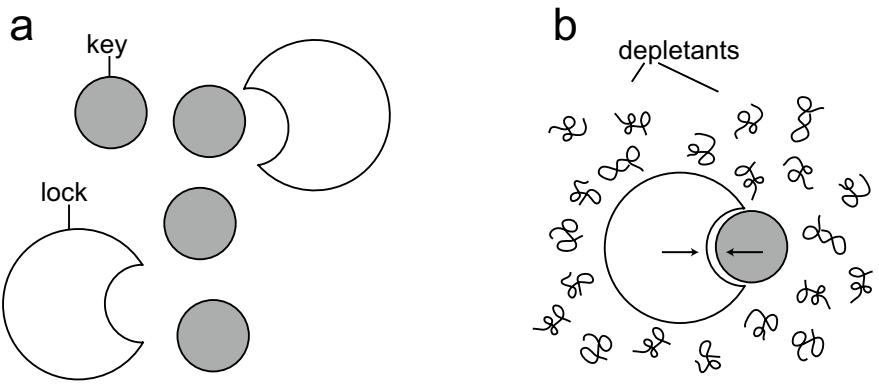

Fig. 11.9 **a** Colloidal 'lock' particles can be synthesised [99] to contain a dimple into which 'key' particles, spherical colloids with appropriate size, can fit. **b** By adding depletants (polymer chains) a key can be pushed into a lock using the depletion force. Inspired by Solomon [100]

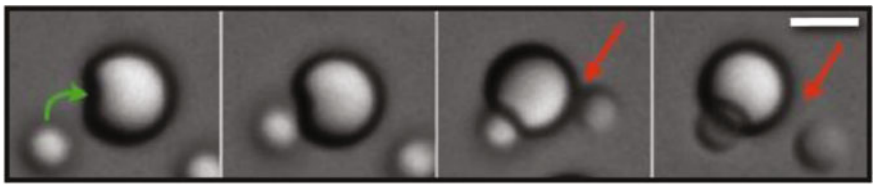

Fig. 11.10 Series of images demonstrating a colloidal sphere entering the lock of larger colloid. The curved arrow in the first micrograph indicates a successful lock–key binding. Scale bar is 2 μm. Reprinted with permission from Ref. [99]. Copyright 2010, Springer Nature

Hence, selecting the strength of the attraction is possible by introducing colloidal surface roughness [106–108]. This makes it possible to direct the self-assembly of particles by selectively controlling the roughness of different sides of colloidal particles. Badaire et al. [109,110] demonstrated the potential of this method in the assembly of lithographically designed colloidal particles. In Fig. 11.12 (left panel) we show the particles used by Badaire et al. [109,110] that consist of roughened, rounded side walls and flat ends. Upon adding surfactant micelles, these particles will attract one another due to the depletion force. Since the attraction is stronger between the flat sides of the particles, rod-like equilibrium structures are formed at a certain depletant concentration. An example of the work of Badaire et al. is depicted in Fig. 11.12 (right panel). Zhao and Mason [106] demonstrated the same principle on plate-like particles with manipulated roughness.

Kraft et al. [111] prepared patchy particles with smooth and rough parts. This made it possible to employ the depletion interaction to make 'colloidal micelles': the patchy particles assemble into clusters that resemble surfactant micelles with the smooth and attractive sides of the colloids located at the interior. Anzini and Parola [108] developed a simple model to describe the effects of surface roughness on the depletion interaction, yielding explicit expressions for a wide range of interesting conditions. The theoretical predictions compare well with the numerical simulations

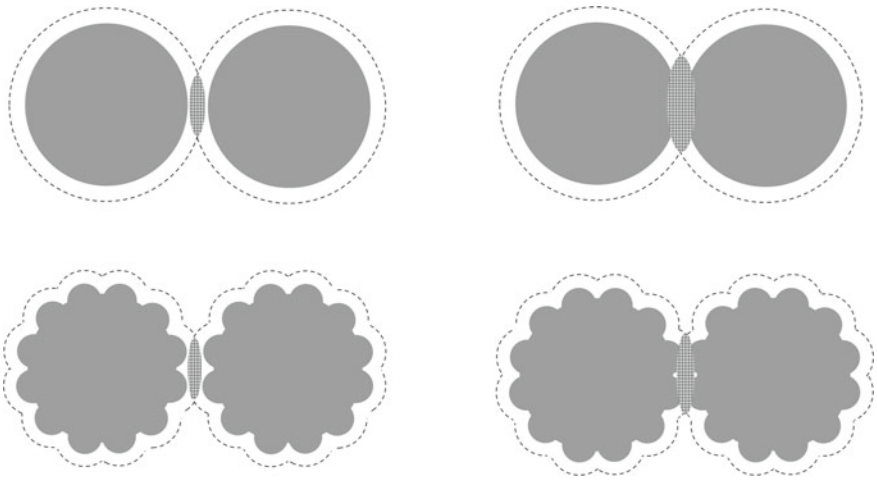

Fig. 11.11 Representation of the overlap zones between two colloidal hard spheres with flat surfaces (*upper*) and two particles with roughened surfaces (*lower*) for small (*left*) and large (*right*) overlap. Drawn by C.M. Martens

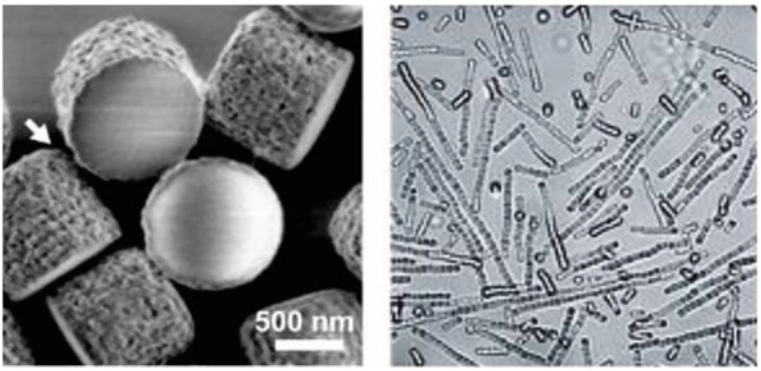

Fig. 11.12 *Left*: Scanning Electron Microscopy (SEM) image of colloidal particles that have sides with surface roughness and smooth sides. *Right*: Aggregated state of these particles under the influence of depletion forces. Image size 50 μm × 50 μm. Reprinted with permission from Refs. [109,110]. Copyright 2007 and 2008 ACS

of Kamp et al. [107]. This theory enables the onset of colloidal aggregation to be predicted in suspensions of rough particles.

In materials science, depletion effects were used in various ways to self-organise colloidal systems. Okabe et al. [112] used it to assemble artificially manufactured components larger than micrometres. By making use of shape complementarity, simple immersion of the microcomponents in polymer solutions enabled assembly.

11.5 Dynamic Depletion Effects

Macromolecular crowding also has consequences for transport properties [113]. One may wonder how protein transport occurs through a cell composed of a highly concentrated dispersion. The viscosity of the cytoplasm will be significantly larger than that of a physiological salt solution. The question arises of what friction a protein experiences as it moves through a cell. This relates to a fundamental problem in colloid physics: the dynamics of a colloidal sphere translating and rotating through a polymer solution.

Dzubiella, Löwen, and Likos [114] considered the flow of a dispersion containing non-interacting Brownian small particles around bigger hard spheres (Fig. 11.13). They found that the effective forces are highly anisotropic. The density profiles are obviously non-trivial. A detailed analysis of the nonequilibrium forces under dynamic circumstances was later performed by Dolata and Zia [115]. A theoretical framework for the non-Newtonian viscosity of a colloidal dispersion with short-ranged depletion attraction was developed by Huang and Zia [116].

As a colloidal particle diffuses or sediments through a solution containing non-adsorbing polymer chains, one may naively expect that the friction experienced by the particle is set by the bulk viscosity. In practice, it is smaller. An analysis of the velocity profile of a nonadsorbing polymer solution near a flat surface shows that depletion leads to effective slip [117]. The depletion layer implies a non-uniform viscosity profile near the surface, which explains this slip. Such effective slip effects also appear when considering the flow of colloidal particles at a wall [118]. Even in the case of simulating colloids in a solvent, the solvent molecules induce deple-

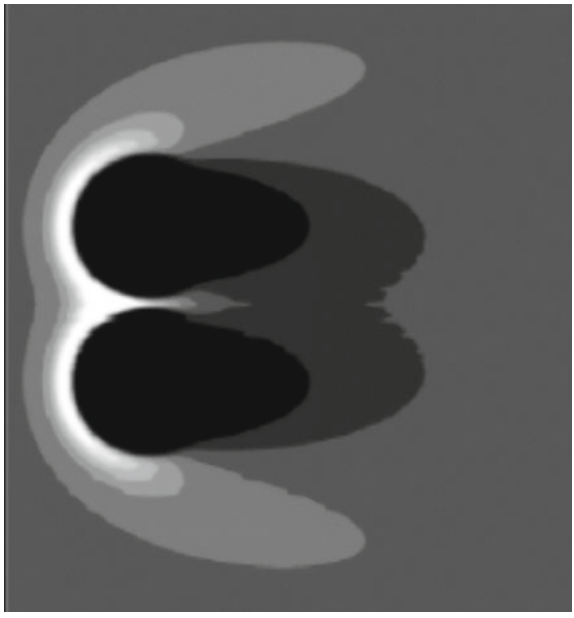

Fig. 11.13 Steady state contour density field (flow from left to right) of Brownian non-interacting spheres around two hard spheres (black). The brighter the region the higher the Brownian particle concentration, which is grey in the bulk (average concentration). Reprinted with permission from Ref. [114]. Copyright 2003 American Physical Society

tion effects [119,120], and it is challenging to properly account for such effects in mesoscale simulation methods.

Phillies and co-workers [121,122] studied the translational self-diffusion of well-defined colloidal spheres through polymer solutions, and showed that the interpretation of the measured friction coefficient of the particles is fairly complicated. For a spherical particle that moves through a medium containing small solvent molecules, the friction coefficient is proportional to the solvent viscosity. When the solvent is replaced by a polymer solution, one may naively expect that the friction coefficient is proportional to the viscosity of the polymer solution. Measurements indicate that this is only true when the chains are very small compared to the size of the particle.

Exercise 11.3. What viscosity is experienced by a tiny sphere in a dilute solution with very long polymer chains?

For polymer chains that are roughly as big as the particle, the apparent or effective viscosity experienced by a sphere is in between the viscosities of solvent and polymer solution. A similar finding was also reported for the rotational diffusion of colloidal particles [123] and for the sedimentation of colloids through a polymer solution [124]. The influence of depletion forces on sedimentation in itself is a rich and challenging topic [125,126].

The fact that the effective viscosity is intermediate between that of solvent and polymer solution can be rationalised as follows. Within the depletion layer, the viscosity is expected to follow the polymer density distribution [117], and it gradually increases from the solvent viscosity at the solid surface to the bulk viscosity far from the particle. Therefore, as a particle diffuses, the hydrodynamic resistance force is also in between the two limits. Fan et al. [127–129] derived analytical expressions for the friction felt by a sphere when it moves through a macromolecular medium and showed that the friction is strongly reduced compared to Stokes' law. This means that depletion-induced slip effects facilitate protein transport through crowded media. This work has been extended to (i) understand the effect of shear flow on the segment density profile of a nonadsorbing polymer solution in a narrow slit [130] and (ii) the mimicking of colloid dynamics of interacting hard spheres mediated by depletants [131,132]. For the diffusion of a slender object through a polymer solution, see Ref. [133].

Krüger and Rauscher [134] calculated the short-time and the long-time diffusion coefficients of a colloidal sphere in a polymer solution and took hydrodynamic interactions into account. It follows that the long-time diffusion coefficient can be described using a generalised Stokes-Einstein relation, whereas it deviates for the short-time coefficient. Ochab and Holyst [135] proposed a model of confined diffusion to describe the diffusion of a sphere through a polymer solution. Their model explains the anomalous diffusion that is observed experimentally [136].

Anomalous diffusive motion of particles in crowded environments such as the interior of cells and in cellular membranes was also evaluated by Höfling and Franosch [137]. For the analysis of anomalous transport, they reviewed the theory that

underlies commonly applied techniques such as single-particle tracking, fluorescence correlation spectroscopy and fluorescence recovery after photobleaching. They show experimental evidence for anomalous transport in crowded biological media. Zöttl and Yeomans [138] investigated the transport of driven nano- and micro-particles in complex fluids. They measured the fluid flow fields and local polymer density and polymer conformation around the particles. Schuler et al. [139] performed extensive single-molecule experiments to investigate the interaction between two intrinsically disordered proteins. They studied the influence of crowding on the association and dissociation kinetics of the proteins and the translational diffusion. Theory by Fan et al. [127,128] can accurately quantify the measured diffusion of proteins through crowded macromolecular media [139,140].

References

1. Grinberg, V.Y., Tolstoguzov, V.B.: Food Hydrocolloids **11**, 145 (1997)
2. Syrbe, A., Bauer, W.K., Kostermeyer, H.: Int. Dairy J. **8**, 179 (1998)
3. Doublier, J.L., Garnier, C., Renard, C., Sanchez, C.: Curr. Opin. Colloid Interface Sci. **5**, 184 (2000)
4. de Kruif, C.G., Tuinier, R.: Food Hydrocolloids **15**, 555 (2001)
5. Overbeek, A., Bückmann, F., Martin, E., Steenwinkel, P., Annable, T.: Progr. Org. Coat. **48**, 125 (2003)
6. Tadros, T.: Colloids in Paints. Wiley (2011)
7. de With, G.: Polymer Coatings. Wiley, New York (2018)
8. Schulz, M., Keddie, J.L.: Soft Matter **14**, 6181 (2018)
9. Baranov, D., Fiore, A., van Huis, M., Giannini, C., Falqui, A., Lafont, U., Zandbergen, H., Zanella, M., Cingolani, R., Manna, L.: Nano Lett. **10**, 743 (2010)
10. Wang, P.Y., Mason, T.G.: Nature **561**, 94 (2018)
11. Marenduzzo, D., Finan, K., Cook, P.R.: J. Cell Biol. **175**, 681–686 (2006)
12. Ping, G., Yang, G., Yuan, J.M.: Polymer **47**, 2564 (2006)
13. Sapir, L., Harries, D.: Curr. Opin. Colloid Interface Sci. **20**, 3 (2015)
14. Secor, P.R., Sweere, J.M., Michaels, L.A., Malkovskiy, A.V., Lazzareschi, D., Katznelson, E., Rajadas, J., Birnbaum, M.E., Arrigoni, A., Braun, K.R., Evanko, S.P., Stevens, D.A., Kaminsky, W., Singh, P.K., Parks, W.C., Bollyky, P.L.: Cell Host Microbe **18**, 549–559 (2015)
15. André, A.A.M., Spruijt, E.: Int. J. Mol. Sci. **21** (2020)
16. Neu, B., Meiselman, H.J.: Biochim. et Biophys. Acta **1760**, 1772 (2006)
17. Stenger, P.C., Zasadzinski, J.A.: Biophys. J. **92**, 3 (2007)
18. Tharmann, R., Claessens, M.M.A.E., Bausch, A.R.: Biophys. J. **90**, 2622 (2006)
19. Dogic, Z., Purdy, K.R., Grelet, E., Adams, M., Fraden, S.: Phys. Rev. E. **69**, 051702 (2004)
20. Hashimoto, S., Yoshida, A., Ohta, T., Taniguchi, H., Sadakane, K., Yoshikawa, K.: Chem. Phys. Lett. **655–656**, 11 (2016)
21. McGuffee, S.R., Elcock, A.H.: PLoS Comput. Biol. **6**, e1000694 (2010)
22. Fulton, A.B.: Cell **30**, 345 (1982)
23. Goodsell, D.S.: Trends Biochem. Sci. **16**, 203 (1991)
24. Ralston, G.B.: J. Chem. Edu. **67**, 857 (1990)
25. Goodsell, D.S.: The Machinery of Life. Springer, New York (1998)
26. Minton, A.P.: Curr. Opin. Struct. Biol. **10**, 34 (2000)
27. Snoussi, K., Halle, B.: Biophys. J. **88**, 2855 (2005)
28. Cheung, M.S., Klimov, D., Thirumalai, D.: Proc. Natl. Acad. Sci. **102**, 4753 (2005)
29. Zimmerman, S.B., Minton, A.P.: Ann. Rev. Biophys. Biomol. Struct. **22**, 27 (1993)
30. Herzfeld, J.: Acc. Chem. Res. **29**, 31 (1996)

31. Ellis, R.J.: Curr. Opin. Struct. Biol. **11**, 114 (2001)
32. Ellis, R.J., Minton, A.P.: Nature **425**, 27 (2003)
33. Ellis, R.J.: Trends Biochem. Sci. **26**, 597 (2001)
34. Walter, H., Brooks, D.E.: FEBS Lett. **361**, 135 (1995)
35. Valkenburg, J.A.C., Woldringh, C.L.: J. Bacteriol. **160**, 1151 (1984)
36. Odijk, T.: Biophys. Chem. **73**, 23 (1998)
37. Woldringh, C.L., Odijk, T.: In: Charlebois, R.L. (Ed.) Organization of the Prokaryotic Genome, Chap. 10. ASM Press, Amsterdam (1999)
38. Iborra, F.J.: Theor. Biol. Med. Mod. **4**, 1 (2007)
39. Hyman, A.A., Brangwynne, C.P.: Dev. Cell **21**, 14 (2011)
40. Hyman, A.A., Weber, C.A., Julicher, F.: Annu. Rev. Cell. Dev. Biol. **30**, 39 (2014)
41. Brangwynne, C.P.: J. Cell Biol. **11**, 899 (2013)
42. Brangwynne, C.P., Tompa, P., Pappu, R.V.: Nat. Phys. **11**, 899 (2015)
43. Mitrea, D.M., Kriwacki, R.W.: Cell Commun. Signal **14**, 1 (2016)
44. Y. Shin, C.P. Brangwynne, Science **357**, eaaf4382 (2017)
45. Banani, H.O., Lee, A.A., Rosen, M.K.: Nat. Rev. Mol. Cell Biol. **18**, 285 (2017)
46. Berry, J., Brangwynne, C.P., Haataja, M.: Rep. Prog. Phys. **81**, 046601 (2018)
47. Sapir, L., Harries, D.: Bunsen-Mag. **19**, 152 (2017)
48. Groen, J., Foschepoth, D., te Brinke, E., Boersma, A.J., Imamura, H., Rivas, G., Heus, H.A., Huck, W.T.S.: J. Am. Chem. Soc. **137**, 13041 (2015)
49. Bernal, J.D., Crowfoot, D.: Nature **133**, 794 (1934)
50. Kendrew, J.C., Bodo, G., Dintzis, H.M., Parrish, R.G., Wyckoff, H., Phillips, D.C.: Nature **181**, 662 (1958)
51. Perutz, M.F., Rossmann, M.G., Cullis, A.F., Muirhead, H., Will, G.: Nature **185**, 416 (1960)
52. Drenth, J.: Principles of Protein X-Ray Crystallography. Springer (2007)
53. Word wide protein data bank: https://www.wwpdb.org/stats/deposition. Accessed 04-08-2023
54. McPherson, A.: J. Cryst. Growth **110**, 1 (1991)
55. McPherson, A.: Methods **34**, 254 (2004)
56. Gilman, J.J. (ed.): The Art and Science of Growing Crystals. Wiley, New York (1963)
57. Drenth, J.: J. Cryst. Growth **90**, 368 (1988)
58. Broide, M.L., Berland, C.R., Pande, J., Ogun, O., Benedek, G.B.: Proc. Natl. Acad. Sci. **88**, 5660 (1991)
59. Berland, C.R., Thurston, G.M., Kondo, M., Broide, M.L., Pande, J., Ogun, O., Benedek, G.B.: Proc. Natl. Acad. Sci. **89**, 1214 (1992)
60. Stradner, A., Schurtenberger, P.: Soft Matter **16**, 307 (2020)
61. Tanaka, T., Ishimoto, C., Chylack, L.T.: Science **197**, 1010 (1977)
62. Ishimoto, C., Tanaka, T.: Phys. Rev. Lett. **39**, 474 (1977)
63. Phillies, G.D.J.: Phys. Rev. Lett. **55**, 1341 (1985)
64. Thomson, J.A., Schurtenberger, P., Thurston, G.M., Benedek, G.B.: Proc. Natl. Acad. Sci. **84**, 7079 (1987)
65. Muschol, M., Rosenberger, F.: J. Chem. Phys. **107**, 1953 (1997)
66. Asherie, N., Lomakin, A., Benedek, G.B.: Phys. Rev. Lett. **77**, 4832 (1996)
67. Rosenbaum, D., Zamora, P.C., Zukoski, C.F.: Phys. Rev. Lett. **76**, 150 (1996)
68. This could be considered as a contribution to the 'Wiedergutmachung' between colloid science in the colloid/macromolecule controversy with protein chemistry [69]
69. Tanford, C., Reynolds, J.: Nature's Robots. Oxford University Press, New York (2001)
70. Poon, W.C.K.: Phys. Rev. E **55**, 3762 (1997)
71. Ten Wolde, P.R., Frenkel, D.: Science **277**, 1975 (1997)
72. Haas, C., Drenth, J.: J. Cryst. Growth **196**, 388 (1999)
73. Galkin, O., Vekilov, P.G.: Proc. Natl. Acad. Sci. **97**, 6277 (2000)
74. Dumetz, A.C., Chockla, A.M., Kaler, E.W., Lenhoff, A.M.: Biophys. J. **94**, 570–583 (2008)
75. Piazza, R.: Curr. Opinion Colloid Interface Sci. **5**, 38 (2000)
76. Kulkarni, A.M., Chatterjee, A.P., Schweizer, K.S., Zukoski, C.F.: Phys. Rev. Lett. **83**, 4554 (1999)

77. Annunziata, O., Asherie, N., Lomakin, A., Pande, J., Ogun, O., Benedek, G.B.: Proc. Natl. Acad. Sci. **99**, 14165 (2002)
78. Annunziata, O., Ogun, O., Benedek, G.B.: Proc. Natl. Acad. Sci. **100**, 970 (2003)
79. Tanaka, S., Ataka, M.: J. Chem. Phys. **117**, 3504 (2002)
80. "see various papers in", Curr. Opinion Colloid Interface Sci. **9**, 1 (2004)
81. Kirner, F., Sturm, E.V.: Cryst. Growth Des. **21**, 5192 (2021)
82. Cohen, S.S.: Proc. Soc. Exp. Biol. Med. **48**, 163 (1941)
83. Li, L.S., Walda, J., Manna, L., Alivisatos, A.P.: Nano Lett. **2**, 557 (2002)
84. Kim, D., Bae, W.K., Kim, S.H., Lee, D.C.: Nano Lett. **19**, 963 (2019)
85. Zhao, C., Wang, G., Takarada, T., Liang, X., Komiyama, M., Maeda, M.: Colloids Surf. A **568**, 216 (2019)
86. Park, K., Koerner, H., Vaia, R.A.: Nano Lett. **10**, 1433 (2010)
87. Mason, T.G.: Phys. Rev. E **66**, 60402 (2002)
88. Piazza, R., Iacopini, S., Pierno, M., Vignati, E.: J. Phys.: Condens Matter **14**, 7563 (2002)
89. Bibette, J.: J. Colloid Interface Sci. **147**, 474 (1992)
90. Ye, X., Millan, J.A., Engel, M., Chen, J., Diroll, B.T., Glotzer, S.C., Murray, C.B.: Nano Lett. **13**, 4980 (2013)
91. Kang, L., Gibaud, T., Dogic, Z., Lubensky, T.C.: Soft Matter **12**, 386 (2016)
92. Bevan, M.A., Ford, D.M., Grover, M.A., Shapiro, B., Maroudas, D., Yang, Y., Thyagarajan, R., Tang, X., Sehgal, R.M.: J. Proc. Contr. **27**, 64 (2015)
93. Dinsmore, A.D., Yodh, A.G., Pine, D.J.: Nature **383**, 239 (1996)
94. Nikoubashman, A., Mahynski, N., Pirayandeh, A., Panagiotopoulos, A.: J. Chem. Phys. **140**, 094903 (2014)
95. Moncho-Jordá, A., Odriozola, G.: Curr. Opin. Colloid Interface Sci. **20**, 24 (2015)
96. Spannuth, M., Conrad, J.C.: Phys. Rev. Lett. **109**, 028301 (2012)
97. Trokhymchuk, A., Henderson, D.: Curr. Opin. Colloid Interface Sci. **20**, 32 (2015)
98. Pandey, R., Conrad, J.C.: Soft Matter **8**, 10695 (2012)
99. Sacanna, S., Irvine, W.T.M., Chaikin, P.M., Pine, D.J.: Nature **464**, 575 (2010)
100. Solomon, M.J., Spicer, P.T.: Soft Matter **6**, 1391 (2010)
101. Wang, Y., Wang, Y., Zheng, X., Yi, G.R., Sacanna, S., Pine, D.J., Weck, M.: J. Am. Chem. Soc. **136**, 6866 (2014)
102. Watanabe, K., Tajima, Y., Shimura, T., Ishii, H., Nagao, D.: J. Colloid Interface Sci. **534**, 81 (2019)
103. Chang, H.Y., Huang, C.W., Chen, Y.F., Chen, S.Y., Sheng, Y.J., Tsao, H.K.: Langmuir **31**, 13085 (2015)
104. Ashton, D.J., Jack, R.L., Wilding, N.B.: Phys. Rev. Lett. **114**, 237801 (2015)
105. Bryk, P., Sokolowski, S.: Appl. Surf. Sci. **253**(13), 5802 (2007)
106. Zhao, K., Mason, T.G.: Phys. Rev. Lett. **99**, 268301 (2007)
107. Kamp, M., Hermes, M., van Kats, C.M., Kraft, D.J., Kegel, W.K., Dijkstra, M., van Blaaderen, A.: Langmuir **32**, 1233 (2016)
108. Anzini, P., Parola, A.: Soft Matter **13**, 5150 (2017)
109. Badaire, S., Cottin-Bizonne, C., Woody, J.W., Yang, A., Stroock, A.D.: J. Am. Chem. Soc. **129**, 40 (2007)
110. Badaire, S., Cottin-Bizonne, C., Stroock, A.D.: Langmuir **24**, 11451 (2008)
111. Kraft, D.J., Ni, R., Smallenburg, F., Hermes, M., Yoon, K., Weitz, D.A., van Blaaderen, A., Groenewold, J., Dijkstra, M., Kegel, W.K.: Proc. Natl. Acad. Sci. **109**, 10787 (2012)
112. Okabe, U., Okano, T., Suzuki, H.: Sens. Actuat. A: Phys. **254**, 43 (2017)
113. Tabaka, M., Kalwarczyk, T., Szymanski, J., Hou, S., Holyst, R.: Front. Phys. **2** (2014)
114. Dzubiella, J., Löwen, H., Likos, C.N.: Phys. Rev. Lett. **91**, 248301 (2003)
115. Dolata, B.E., Zia, R.N.: J. Fluid Mech. **836**, 694–739 (2018)
116. Huang, D.E., Zia, R.N.: J. Colloid Interface Sci. **562**, 293 (2020)
117. Tuinier, R., Taniguchi, T., Phys, J.: Condens. Matter **17**, L9 (2005)
118. Ghosh, S., van den Ende, D.T.M., Mugele, F., Duits, M.H.G.: Colloids Surf. A **491**, 50 (2016)
119. Wagner, M., Ripoll, M.: Int. J. Mod. Phys. C **30**, 1941008 (2019)

120. Barcelos, E.I., Khani, S., Boromand, A., Vieira, L.F., Lee, J.A., Peet, J., Naccache, M.F., Maia, J.: Comput. Phys. Commun. **258**, 107618 (2021)
121. Lin, T.H., Phillies, G.D.J.: J. Phys. Chem. **86**, 4073 (1982)
122. Ullmann, G.S., Ullmann, K., Lindner, R.M., Phillies, G.D.J.: J. Phys. Chem. **89**, 692 (1985)
123. Koenderink, G.H., Sacanna, S., Aarts, D.G.A.L., Philipse, A.P.: Phys. Rev. E **69**, 021804 (2004)
124. Ye, X., Tong, P., Fetters, L.J.: Macromolecules **31**, 5785 (1998)
125. Lattuada, E., Buzzaccaro, S., Piazza, R.: Phys. Rev. Lett. **116**, 038301 (2016)
126. Fiore, A.M., Wang, G., Swan, J.W.: Phys. Rev. Fluids **3**, 063302 (2018)
127. Tuinier, R., Dhont, J.K.G., Fan, T.H.: Europhys. Lett. **75**, 929 (2006)
128. Fan, T.H., Dhont, J.K.G., Tuinier, R.: Phys. Rev. E. **75**, 018803 (2007)
129. Fan, T.H., Xie, B., Tuinier, R.: Phys. Rev. E. **76**, 051405 (2007)
130. Taniguchi, T., Arai, Y., Tuinier, R., Fan, T.H.: Eur. Phys. J. E **35**, 88 (2012)
131. Karzar-Jeddi, M., Tuinier, R., Taniguchi, T., Fan, T.H.: J. Chem. Phys. **140**, 214906 (2014)
132. He, Y., Li, L., Taniguchi, T., Tuinier, R., Fan, T.H.: Phys. Rev. Fluids **5**, 013302 (2020)
133. Morozov, K.I., Leshansky, A.M.: Macromolecules **55**, 3116–3128 (2022)
134. Krüger, M., Rauscher, M.: J. Chem. Phys. **131**, 094902 (2009)
135. Ochab-Marcinek, A., Hołyst, R.: Soft Matter **7**, 7366 (2011)
136. Kalwarczyk, T., Sozanski, K., Ochab-Marcinek, A., Szymanski, J., Tabaka, M., Hou, S., Holyst, R.: Adv. Colloid Interface Sci. **223**, 55 (2015)
137. Höfling, F., Franosch, T.: Rep. Progr. Phys. **76**, 046602 (2013)
138. Zöttl, A., Yeomans, J.M.: J. Phys.: Condens. Matter **31**, 234001 (2019)
139. Zosel, F., Soranno, A., Buholzer, K.J., Nettels, D., Schuler, B.: Proc. Natl. Acad. Sci. **117**, 13480 (2020)
140. Galvanetto, N., Ivanovic, M., Chowdhury, A., Sottini, A., Nüesch, M., Nettels, D., Best, R., Schuler, B.: Nature **619**, 876 (2023)